CHIN. PHYS. LETT. Vol. 37, No. 6 (2020) 064204

Switching between the Functions of Half-Wave Plate and Quarter-Wave Plate Simply by Using a Vanadium Dioxide Film in a Terahertz Metamaterial *

Jian-Xing Zhao(赵建行)[1], Jian-Lin Song(宋建林)[1], Yao Zhou(周姚)[1], Yi-Chao Liu(刘艺超)[1], Jian-Hong Zhou(周见红)[1,2]**

[1]School of Photoelectric Engineering, Changchun University of Science and Technology, Changchun 130022, China
[2]Key Laboratory of Optoelectric Measurement and Optical Information Transmission Technology (Ministry of Education), Changchun University of Science and Technology, Changchun 130022, China

(Received 5 March 2020)

We propose a switchable THz metamaterial that can be switched between two functions of half-wave plate and quarter-wave plate. The two switchable functions can be simply achieved by inserting a VO_2 film in the metamaterial design. Finite-difference time-domain (FDTD) simulation results show that the proposed metamaterial can convert x-polarized incident wave to y-polarized reflected wave when VO_2 is at metal phase, and convert x-polarized wave to circularly polarized wave when VO_2 is at insulator phase. The metamaterial performs well in the two functions, i.e., the same broad working frequency band and near perfect polarization conversion. The switching effect originates from the switchable Fabry–Pérot cavity length induced by the phase change of VO_2. We believe that our findings provide a reference in designing switchable metamaterials.

PACS: 42.79.Ci, 42.25.Ja, 78.20.Bh DOI: 10.1088/0256-307X/37/6/064204

During the past decade, metamaterials have drawn a great deal of attention from the scientific community. As an artificial material, metamaterials possess many novel properties such as asymmetric transmission,[1–4] polarization conversion,[5–7] and perfect absorption.[8,9] One can obtain any of the functions at will through appropriate design. Recent research on metamaterials focused on their tunable properties. However, once fabricated, it is difficult to tune a metamaterial. To overcome this issue, additional processes such as reversible electrochemical deposition[10] and using stretchable substrate[11] are proposed to acquire a tunable spectrum of the metamaterial. Tunable materials such as graphene[12–15] and Dirac semimetal[16–20] are also considered in metamaterial design. These metamaterials usually possess the tunable working frequency or intensity for one single function. Most recently, vanadium dioxide (VO_2) that possesses reversible insulator-to-metal phase transition is being widely studied. The phase transition can be achieved through various external stimuli such as thermal heating,[21] applied current[22] and optical pumping.[23,24] VO_2 integrated metamaterials are widely reported to achieve switchable functions such as perfect absorption, polarization conversion and electromagnetically induced transparency effects[25–28] due to their insulator-to-metal transitions at the temperature of 358 K.[25] However, most of these works used hybrid metal-VO_2 antenna or multilayered antenna to acquire switchable functions, which could complicate the fabrication process of metamaterials.

In this Letter, we propose a design method of simply inserting a VO_2 film into a THz metamaterial to achieve switching between two functions of half-wave plate and quarter-wave plate. The designed metamaterial consists of a gold antenna layer, a VO_2 film and a gold substrate separated by dielectric spacers. Finite-difference time-domain (FDTD) simulation results show that when VO_2 is at metal phase, the x-polarized incident wave can be well converted to a y-polarized reflected wave over a broad band of from 2.0 THz to 2.4 THz, when VO_2 is at insulator phase, the x-polarized incident wave can be converted to a circularly polarized reflected wave with a less than 3 dB axis ratio over the frequency bands of from 1.65 THz to 2.58 THz and from 2.9 THz to 2.96 THz. We also investigate the working mechanism of the switching process and attribute that to the switching of the Fabry–Pérot length induced by the phase change of VO_2 film. The impacts of the geometric parameters of the metamaterial on the converting performance are also analyzed.

The schematic diagram of the proposed metamaterial is shown in Fig. 1. Figure 1(a) shows the top view of the unit cell, where the rectangular gold antenna is on the surface of the metamaterial, oriented at 45° with respect to the x-axis. Figure 1(b) shows the cross-sectional view of the unit cell, from which we can see that the metamaterial consists of an antenna layer, a VO_2 film and a gold substrate. The three layers are separated by polyethylene cyclic olefin copolymer (TOPAS) spacers due to its low absorption in THz regime.[29] In our design, the conductivity of the gold antenna is $\sigma = 4 \times 10^7$ S/m.[30] The refractive index of the TOPAS polymer is about 1.53.[29] VO_2 is modeled as a phase change material. Its metal phase is modeled by the frequency-independent conductivity of $\sigma = 2 \times 10^5$ S/m, and its insulator phase is modeled by a dielectric permittivity of 12 with a

*Supported by the Scientific and Technological Developing Scheme of Jilin Province (Grant No. 20180101281JC), "135" Research Project of Education Bureau of Jilin Province (Grant No. JJKH20190579KJ), and "111" Project of China (Grant No. D17017).
**Corresponding author. Email: zjh@cust.edu.cn
© 2020 Chinese Physical Society and IOP Publishing Ltd

conductivity of $\sigma = 0\,\mathrm{S/m}$.[25] The thicknesses of the antenna layer, the VO_2 film and the gold substrate are 0.2 μm, 1 μm and 2 μm, respectively. The geometric parameters shown in Figs. 1(a) and 1(b) are $a = 40\,\mu\mathrm{m}$, $b = 30\,\mu\mathrm{m}$, $p = 86\,\mu\mathrm{m}$, $t_1 = 11.8\,\mu\mathrm{m}$ and $t_2 = 7.2\,\mu\mathrm{m}$, respectively.

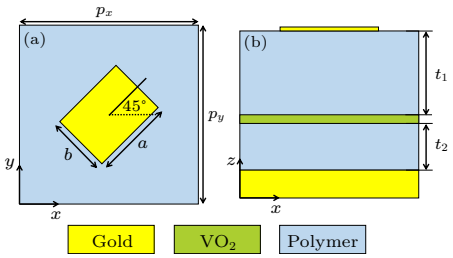

Fig. 1. (a) Top view and (b) cross-sectional view of the unit cell of the proposed metamaterial.

In order to numerically investigate the performance of the proposed metamaterial, we performed the simulation using the finite-difference time-domain software (Lumerical FDTD solutions) to calculate the polarization conversion characteristics and plasmonic mode properties. In our simulations, perfectly matched layer (PML) boundary conditions are applied in the $\pm z$ directions to mimic a infinite space due to the near perfect absorption of light waves. Periodic boundary conditions are applied in the x- and y-directions. An x-polarized plane wave source that is 130 μm away from the metamaterial surface is normally incident from $+z$ direction to $-z$ direction, with a primary phase of zero. The monitor is placed at 145 μm away from the metamaterial surface to detect the amplitude and phase of the reflected wave. The mesh sizes along x, y and z directions are 1 μm, 1 μm and 0.06 μm, respectively. To characterize the polarization relation of the complex amplitudes of the reflected and the incident waves, we use the 2×2 scattering matrix[31]

$$R = \begin{pmatrix} R_{xx} & R_{xy} \\ R_{yx} & R_{yy} \end{pmatrix}, \tag{1}$$

with x and y being the linear polarization states of the reflected and incident waves. In our analysis we also utilize the Stokes parameters[32]

$$I = |R_{xx}|^2 + |R_{yx}|^2, \tag{2}$$

$$Q = |R_{xx}|^2 - |R_{yx}|^2, \tag{3}$$

$$U = 2\,|R_{xx}|\,|R_{yx}|\cos\Delta\phi, \tag{4}$$

$$V = 2\,|R_{xx}|\,|R_{yx}|\sin\Delta\phi, \tag{5}$$

where $\Delta\phi$ represents the phase difference between x and y polarizations. For the half-wave plate, the x-polarized incident wave can be converted to a y-polarized reflected wave, and the polarization conversion ratio (PCR) can be defined as[17]

$$\mathrm{PCR} = \frac{|R_{yx}|^2}{|R_{xx}|^2 + |R_{yx}|^2}. \tag{6}$$

For the quarter wave plate, the x-polarized incident wave can be converted to a circularly polarized reflected wave, and the axis ratio (AR)

$$\mathrm{AR} = 10\log(\tan\beta) \tag{7}$$

($\sin(2\beta) = V/I$, with β being the ellipticity angle) and ellipticity (V/I) can be utilized to quantify the circular polarization performance. The conversion efficiency can be expressed as

$$\eta = |R_{xx}|^2 + |R_{yx}|^2. \tag{8}$$

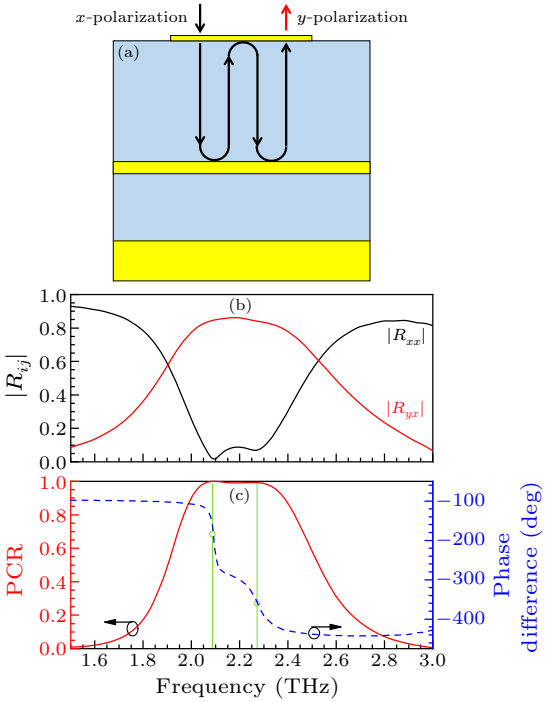

Fig. 2. (a) Schematic of the working process when VO_2 is at metal phase. (b) Moduli of the scattering components for x-polarization incidence. (c) Calculated PCR and phase difference of x- and y-components of electric field.

When the temperature is 358 K, VO_2 transmits to its metal phase. The VO_2 film acts as a reflection mirror and, as shown in Fig. 2(a), the proposed metamaterial can convert x-polarized incident wave to y-polarized reflected wave. We present the moduli $|R_{ij}|$ of the scattering matrix components for x-polarization incidence in Fig. 2(b). From Fig. 2(b) we can see that, in a broad frequency band of about 2.0 THz to 2.4 THz, the co-polarization reflection coefficient $|R_{xx}|$ (the red curve) is nearly zero and the cross-polarization reflection coefficient $|R_{yx}|$ (the black curve) is high, indicating that the x-polarized is mostly converted to a y-polarized reflected wave. The conversion efficiency PCR calculated from Eq. (6) is shown by the solid curve in Fig. 2(c), which performs a near unity PCR in the frequency band of interest. Especially at the frequencies of 2.09 THz and 2.27 THz, the PCRs are 0.999 and 0.993, and the phase differences $\Delta\phi$ ($\phi_x - \phi_y$ see the dashed curve in Fig. 2(c)) are $-180°$ and $-360°$, indicating a near perfect half-wave plate.

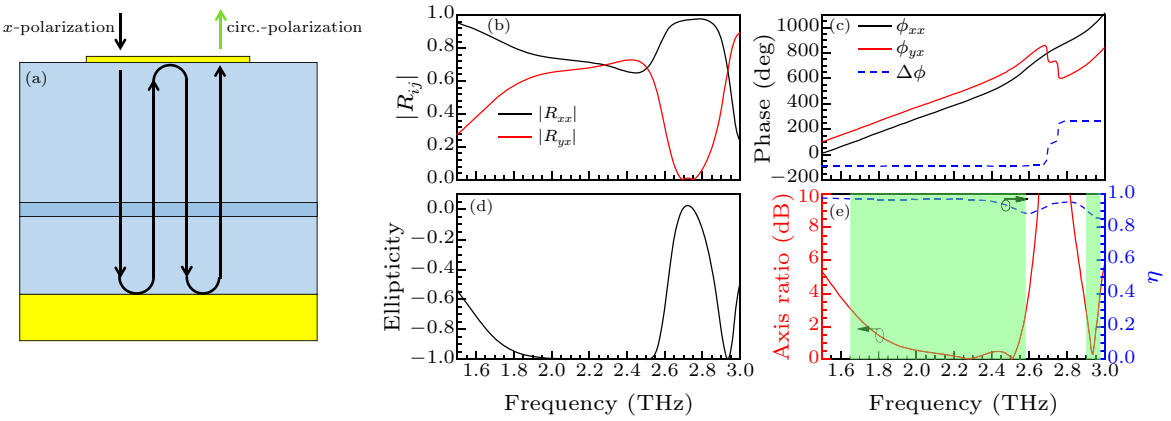

Fig. 3. (a) Schematic of the working process when VO_2 is at insulator phase. (b) Moduli of the scattering components for x-polarization incidence. (c) The phase response and phase difference of x- and y-components. (d) Ellipticity for x-polarization incidence. (e) The axis ratio and conversion efficiency of the metamaterial.

When the temperature is 298 K (room temperature), VO_2 transmits to its insulator phase. The VO_2 film is transparent for THz wave[25] as shown in Fig. 3(a), and the proposed metamaterial can convert an x-polarized incident wave to a circularly polarized reflected wave. Figure 3(b) shows the magnitude of the reflected x- and y-components of electric field (scattering matrix components), from which we can see that the difference between the two components is less than 0.2 over the frequency ranges 1.65–2.58 THz and 2.9–2.96 THz. The phase difference between the two components is about $-90°$ or $270°$, as shown in Fig. 3(c). Figure 3(d) shows the calculated ellipticity (V/I) by using the Stokes parameters. We can see that the ellipticity is nearly -1 in the two interested frequency bands, which means that a left-hand circularly polarized wave[32] is acquired. Then, using Eqs. (7) and (8), we calculate the axis ratio and converting efficiency of the metamaterial and plot them in Fig. 3(e). Over the frequency ranges 1.65–2.58 THz and 2.9–2.96 THz (the green regions), the axis ratio is below 3 dB and the efficiency is higher than 0.85, indicating a good performance of the quarter-wave plate.

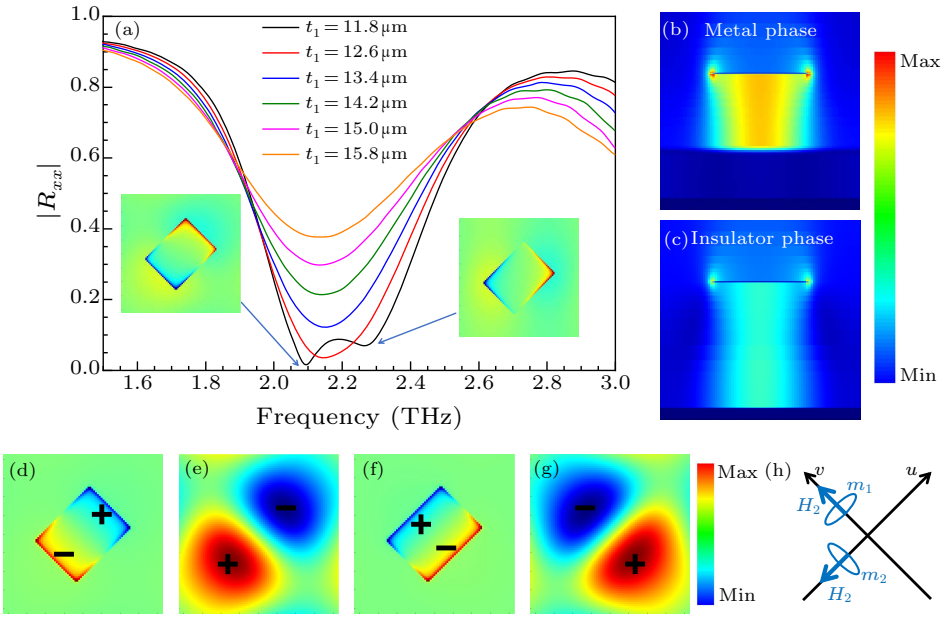

Fig. 4. (a) The co-polarization coefficient $|R_{xx}|$ with different values of t_1. The magnitude of magnetic field distributions on the x–z plane at the frequency of 2.09 THz when VO_2 is at (b) metal phase and (c) insulator phase. The z-component electric field distributions of [(d), (f)] the lower surface of antenna, [(e), (g)] the upper surface of the substrate, for [(d), (e)] u-polarized incidence and [(f), (g)] v-polarized incidence at 2.27 THz.

Then, we investigate the physical mechanism of the switching process. We first plot the co-polarization coefficient $|R_{xx}|$ of the original structure (the black curve) when VO_2 is at metal phase in Fig. 4(a). In this case, the x-polarized incident wave is almost all converted to a y-polarized reflected wave at the two frequencies of 2.09 THz and 2.27 THz. We attribute the perfect polarization conversion effect to two contributors, the resonance antenna on the surface of the metamaterial and the Fabry–Pérot cavity in the metal-

insulator-metal structure. The z-component electric field distributions on the antenna at the two frequencies are shown in the insets of Fig. 4(a), which are dipole resonances with the moment directions deviating from the incident polarization direction to contribute to the polarization conversion.[14,17,31] Then, with the assistance of the well designed Fabry–Pérot cavity ($t_1 = 11.8\,\mu$m), the wave interacts with the resonance antenna many times, resulting in the enhancement of the polarization conversion effect.[12,33] Thus, the near perfect polarization conversion function like a half-wave plate can be achieved. If we increase the length of the Fabry–Pérot cavity t_1, the Fabry–Pérot resonance will undergo a red shift[34] and no longer match the polarization conversion frequency, leading to the weakening of the polarization conversion effect and the increase of the co-polarization coefficient $|R_{xx}|$, as shown in Fig. 4(a). Therefore, when VO_2 transits to the insulator phase, the VO_2 film is transparent, and another Fabry–Pérot cavity is formed by the antenna layer and the gold substrate. The Fabry–Pérot cavity is lengthened and the polarization rotation is weakened. Figures 4(b) and 4(c) show the magnitude of the magnetic field distributions on the x–z plane at the frequency of 2.09 THz when VO_2 is at metal phase and insulator phase, respectively. We can see that the magnetic field at metal phase is stronger than that of the insulator phase due to the stronger Fabry–Pérot resonance, which further validates our analysis.

For the function of quarter-wave plate, taking the frequency of 2.27 THz as an example, we present the electric field distributions on the lower surface of the antenna and the upper surface of the gold substrate in the u–v coordinate system[32] in Figs. 4(d)–4(g). The charge distributions derived from the electric field distributions show that the magnetic resonances are formed for both the u-polarization incidence (Figs. 4(d) and 4(e)) and v-polarization incidence (Figs. 4(f) and 4(g)) by current loops. The equivalent magnetic moments m_1 and m_2 shown in Fig. 4(h) manipulate the magnitudes and phases of the reflected electric fields along the u and v axes, respectively. If the u-component and v-component of the reflected electric fields have equal magnitudes and a phase difference of 90°, the function of a quarter-wave plate will be achieved. Therefore for x-polarization incidence, after optimal design of $t_2 = 7.2\,\mu$m, the reflected wave possesses the approximation of a circular polarization, i.e., $|R_{xx}| = |R_{yx}|$ and $\Delta\phi = 2n\pi \pm \pi/2$. Thus, the function of a quarter-wave plate can be achieved by the proposed metamaterial.

In addition, we investigate the performance of the proposed metamaterial with different geometric parameters. Figures 5(a) and 5(b) show the PCR (metal phase) and ellipticity (insulator phase) with different values of p. For the metal phase, when p increases from 78 μm to 94 μm, the PCR peak undergoes a split with the high PCR band nearly unchanged, similarly for the insulator phase, two pass bands that possess good performance of circular polarization conversion (ellipticity nearly −1) gradually arise. Figures 5(c) and 5(d) show the PCR and ellipticity change with the antenna length. For the metal phase, as shown in Fig. 5(c), when a decreases from 40 μm to 32 μm, the PCR peak value decreases a lot. This is because the decrease of length a will lead to the decrease of the deviation of the dipole moment from the incident polarization direction and further decrease the polarization conversion effect. When a increases from 40 μm to 48 μm, i.e., the length along the long axis of the antenna is increasing, the dipole resonance along the long axis undergoes a red shift and leads to the red shift of the PCR peak at the lower frequency. For the insulator phase, as shown in Fig. 5(d), the 4 μm change in antenna length a has strong influence on the ellipticity, which should be taken care of in the fabrication process. We also investigate the influence of t_2 on the performance of the metamaterial. At the metal phase, because the wave is blocked by the metallic VO_2 film, the change in t_2 has no influence on the PCR value as shown in Fig. 5(e). While at the insulator phase, the influence of t_2 value on the ellipticity cannot be neglected and, as shown in Fig. 5(f), a good performance of quarter-wave plate (broader band and closer to −1) can be acquired when $t_2 = 7.2\,\mu$m.

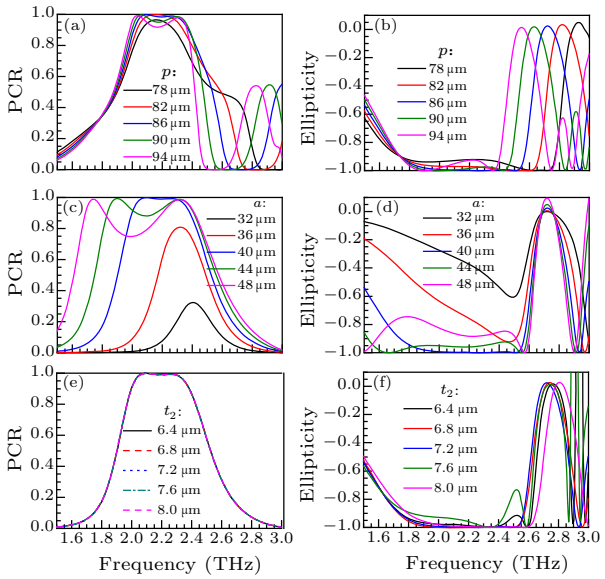

Fig. 5. The PCR [(a), (c), (e)] at metal phase and ellipticity [(b), (d), (f)] at the insulator phase with different values of p, a and t_2.

In summary, we have proposed a VO_2 integrated metamaterial that can be switched between two functions of half-wave plate and quarter-wave plate. The switching function is realized simply by using the VO_2 film. The numerical results show that the proposed metamaterial can convert x-polarized incident THz wave to y-polarized reflected wave when VO_2 is at metal phase, and convert x-polarized incident wave to circularly polarized wave when VO_2 is at insulator phase. Both the converting functions perform well over broad frequency bands. The origin of the switch-

ing effect is the switchable length of Fabry–Pérot cavity induced by the phase change of VO_2. We believe that our findings may serve as a reference to the field of switchable metamaterials.

References

[1] Menzel C, Helgert C, Rockstuhl C, Kley E B, Tunnermann A, Pertsch T and Lederer F 2010 *Phys. Rev. Lett.* **104** 253902
[2] Shi J H, Liu X C, Yu S W, Lv T T, Zhu Z, Ma H F and Cui T C 2013 *Appl. Phys. Lett.* **102** 191905
[3] Zhao J, Fu Y, Liu Z and Zhou J 2017 *Opt. Express* **25** 23051
[4] Li T, Hu F, Qian Y, Xiao J, Zhang L, Zhang W and Han J 2020 *Chin. Phys. B* **29** 024203
[5] Floess D, Chin J Y, Kawatani A, Dregely D, Habermeier H, Weiss T and Giessen H 2015 *Light: Sci. & Appl.* **4** e284
[6] Yang C, Luo Y, Guo J, Pu Y, He D, Jiang Y, Xu J and liu Z 2016 *Opt. Express* **24** 16913
[7] Pu Y, Luo Y, Liu L, He D, Xu H, Jing H, Jiang Y and Liu Z 2018 *Chin. Phys. B* **27** 024202
[8] Yao G, Ling F, Yue J, Luo C, Ji J and Yao J 2016 *Opt. Express* **24** 1518
[9] Luo J and Lin Y 2019 *Appl. Phys. Lett.* **114** 051601
[10] Wang G, Chen X, Liu S, Wang C and Chu S 2016 *ACS Nano* **10** 1788
[11] Song S, Ma X, Pu M, Li X, Liu K, Cao P, Zhao Z, Wang Y, Wang C and Luo X 2017 *Adv. Opt. Mater.* **5** 1600829
[12] Zhao J, Song J, Xu T, Yang T and Zhou J 2019 *Opt. Express* **27** 9773
[13] Zhu L, Liu F, Lin H, Hu J, Yu Z, Wang X and Fan S 2016 *Light: Sci. & Appl.* **5** e16052
[14] Guo T and Argyropoulos C 2016 *Opt. Lett.* **41** 5592
[15] Zeng B, Huang Z, Singh A, Yao Y, Azad A K, Mohite A D, Taylor A J, Smith D R and Chen H 2018 *Light: Sci. & Appl.* **7** 51
[16] Liu G D, Zhai X, Meng H Y, Lin Q, Huang Y, Zhao C J and Wang L L 2018 *Opt. Express* **26** 11471
[17] Zhao J X, Song J L, Zhou Y, Zhao R L and Zhou J H 2019 *IEEE Photon. J.* **11** 4601709
[18] Meng H, Shang X, Xue X, Tang K, Xia S, Zhai X, Liu Z, Chen J, Li H and Wang L 2019 *Opt. Express* **27** 31062
[19] Luo J, Lin Q, Wang L, Xia S, Meng H and Zhai X 2019 *Opt. Express* **27** 20165
[20] Dai L, Zhang Y, O'Hara J F and Zhang H 2019 *Opt. Express* **27** 35784
[21] Wang D, Zhang L, Gu Y, Mehmood M Q, Gong Y, Srivastava A, Jian L, Venkatesan T, Qiu C and Hong M 2015 *Sci. Rep.* **5** 15020
[22] Zhao S, Hu F, Xu X, Jiang M, Zhang W, Yin S and Jiang W 2019 *Chin. Phys. B* **28** 054203
[23] Guo P, Wermer M S, Emery J D, Diroll B T, Chen X, Hock A S, Chang R P H, Martinson A B F and Schaller R D 2017 *ACS Nano* **11** 693
[24] Cai H, Chen S, Zou C, Huang Q, Liu Y, Hu X, Fu Z, Zhao Y, He H and Lu Y 2018 *Adv. Opt. Mater.* **6** 1800257
[25] Ding F, Zhong S and Bozhevolnyi S I 2018 *Adv. Opt. Mater.* **6** 1701204
[26] Song Z, Chen A, Zhang J and Wang J 2019 *Opt. Express* **27** 25196
[27] He H, Shang X, Xu L, Zhao J, Cai W, Wang J, Zhao C and Wang L 2020 *Opt. Express* **28** 4563
[28] Song Z, Chen A and Zhang J 2020 *Opt. Express* **28** 2037
[29] Cunningham P D, Valdes N N, Vallejo F A, Hayden L M, Polishak B, Zhou X, Luo J, Jen A K Y, Williams J C and Twieg R J 2011 *J. Appl. Phys.* **109** 043505
[30] Zhang Y, Feng Y, Jiang T, Cao J, Zhao J and Zhu B 2018 *Carbon* **133** 170
[31] Luo S, Li B, Yu A, Gao J, Wang X and Zuo D 2018 *Opt. Commun.* **413** 184
[32] Dai L, Zhang Y, Guo X, Zhao Y, Liu S and Zhang H 2018 *Opt. Mater. Express* **8** 3238
[33] Wang Y, Jin R, Li J, Li J and Dong Z 2018 *Opt. Express* **26** 3508
[34] Jing X, Gui X, Zhou P and Hong Z 2018 *J. Lightwave Technol.* **36** 2322